Full paper

LMI-based Multiobjective Integral Sliding Mode Control for Rotary Inverted Pendulum System Under Load Variations

Fairus, M. A.[a], Mohamed, Z.[b], Ahmad, M. N.[b], Loi, W. S.[c]

[a]Department of Control, Instrumentation & Automation, Faculty of Electrical Engineering, Universiti Teknikal Malaysia Melaka, Hang Tuah Jaya, 76100 Durian Tunggal, Melaka, Malaysia
[b]Department of Control and Mechatronic Engineering, Faculty of Electrical Engineering, Universiti Teknologi Malaysia, 81310 UTM Johor Bahru, Johor, Malaysia
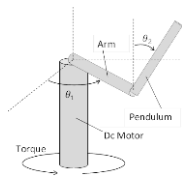[c]Department of Power Electronics & Drives, Faculty of Electrical Engineering, Universiti Teknikal Malaysia Melaka, Hang Tuah Jaya, 76100 Durian Tunggal, Melaka, Malaysia

*Corresponding author: mfairus@utem.edu.my

Graphical abstract

Abstract

This paper presents a multiobjective integral sliding mode controller (ISMC) for a rotary inverted pendulum system under the influence of varying load. Firstly, the nonlinear system is approximated to facilitate the desired control design via extended linearization and deterministic approach. By using both of these techniques, the nonlinear system is formulated into a nonlinear state-space representation where the uncertainties are retained in the model. Next, the design objectives are formulated into linear matrix inequalities (LMI) which are then solved efficiently through convex optimization algorithms. With proper selection variables, numbers of the decision variables for LMIs are reduced. Hence, it will reduce the numerical burden and believes the calculated values more viable in practice. Finally, simulation works are conducted and comparison is made between the proposed controller, such as normal ISMC and LQR. The simulation results illustrate the effectiveness of the proposed controller and the performance is evaluated through integral of absolute-value error (IAE) performance index.

Keywords: Integral sliding mode; multiobjective; linear matrix inequality; rotary inverted pendulum; extended linearization

■1.0 INTRODUCTION

The rotary inverted pendulum system or Furuta pendulum system is a classical control problem used to stabilize an inherently nonlinear, under-actuated, non-minimum phase and unstable system [1]. Typically, this system was composed of a pendulum, rotating arm, motor and encoders where the arm is revolved through driving motor and it controls the motion of the pendulum. The fundamental control objective of the rotary inverted pendulum system is to control the arm motion such that the pendulum is stabilized around the unstable equilibrium point (the upright position).

The model of the rotary inverted pendulum system can be obtained through several methods including the Newton-Euler approach and Euler-Lagrange approach with the latter is the most commonly used approach [2, 3]. Many researchers found that disturbances and uncertainties in the model due to viscous friction at the arm and pendulum, Coulomb friction and backlash [4–6]. However, they found less research works that covers the model with parametric uncertainties that cause by varying load mounted at the pendulum. With load at a free end of the pendulum, center of mass and moment inertia of the pendulum had affected. These values change based on the weight of the applied load. In this work, the effect of the load considered and this model derived by using Euler-Lagrange approach and taking the varying load as the system uncertainties.

Extended linearization, apparent linearization or SDC parameterization are a process for factorizing a nonlinear system into a linear-like structure which contains SDC matrices [7–9]. It treats the SDC matrices as constant and uses a linear control structure to produce a closed loop SDC matrix which is pointwise Hurwitz. Extended linearization known for its non-unique form which creates extra degrees of freedom that used to enhance controller performance [9, 10]. Several research finding had been found and discussed such as in [10–13]. Most of the studies are revolved around the state feedback controller structure since the developed model is in a linear-like structure. In this study, the dynamics model of the rotary inverted pendulum system is factorized using the extended linearization method. Based on the extended linearization, it will reduce the nonlinear system to a linear-like structure which has large pointwise controllability in the region of operation. However, the combination of

deterministic approach, the model obtained will retain the uncertainties of the system in the form of nonlinear model [14] where the model is decomposed into its nominal and uncertainties part. Thus, instead of a linear-like state space representation the obtained model is a state space model with uncertainties.

Variable structure based controller is one of proposed control technique to control the rotary inverted pendulum system. Specifically, this used an integral sliding mode control as the variable structure based controller. In this paper, a multiobjective integral sliding mode controller proposed to solve the regulator problem of the rotary inverted pendulum system under the influence of varying load. A LMI approach used for multiple design objectives. The considered design objectives are optimizing the control effort by minimization of a quadratic cost function and constraining the location of the closed-loop poles within a specified LMI region such that the control system are guaranteed stable and satisfies the desired transient response. These objectives are formulated in terms of LMIs constraints and are solved efficiently through convex optimization algorithms. In this work the decision variables of the LMIs constraints are reduce into a single variable whereas other works as discussed in [15–17] consists of multiple decision variables. By reducing the number of the decision variables, the numerical burden is reduced but at the cost of conservatism [18]. Thus, the results obtained may be efficient in practice.

This paper is organized into seven sections. The next section defines the class of continuous-time uncertain nonlinear system that to be considered and the design objectives. Section 3 discusses the stability of the closed-loop system during sliding mode and the formulation of the design objectives into LMIs. In Section 4, proposed the LMI-based integral sliding mode controller and its reachability condition. Section 5, formulates the dynamic equation of the rotary inverted pendulum system under various load condition based on the combination of extended linearization and deterministic approach. In Section 6, simulation results are presented to support the theoretical analysis of the proposed controller. Some concluding remarks are presented in Section 7.

■2.0   MODEL DESCRIPTION

This paper deals with multiobjective integral sliding mode control for continuous-time uncertain nonlinear system. The nonlinear system is given as

$$\dot{x}(t) = f(x, \varsigma, t) + B(x, \varsigma, t)u(t) \qquad (1)$$

where $x(t) \in \mathbb{R}^n$ known as system state, $u(t) \in \mathbb{R}^m$ denotes as control input, ς is uncertainties causes by known parameters variations, $f(.)$ and $B(.)$ are continuous nonlinear functions with appropriate dimensions.

To begin, the nonlinear system (1) will transformed into a state-space representation of uncertain nonlinear system that based on the idea of extended linearization with state-dependent coefficient (SDC) matrices and deterministic approach.

The extended linearization is a process to factorize a nonlinear system into a linear-like structure which contains SDC matrices. Extended linearization created extra degrees of freedom that enhance controller performance. To achieve this, a proper selection of a vector of free design parameter had to be done such that the nonlinear system (1) can be factored as

$$\dot{x}(t) = A(x, \varsigma, \zeta, t)x(t) + B(x, \varsigma, t)u(t) \qquad (2)$$

where ζ is the vector of free design parameter which it can be selected to have any finite real value, but is generally chosen in the range $[0,1]$.

Next, the associated with the extended linearization form (2) and given a bounded open set $\Omega \subseteq \mathbb{R}^n$, the pair $\{A(x, \varsigma, \zeta, t), B(x, \varsigma, t)\}$ is controllable (stabilizable) parameterization of the nonlinear system (1) in region Ω if $\{A(x, \varsigma, \zeta, t), B(x, \varsigma, t)\}$ is pointwise controllable (stabilizable) in the linear sense for all $x \in \Omega$.

Unlike the extended linearization as discussed in [8, 9], [19] with the deterministic approach, the constructed dynamic equation in this research will retains the nonlinear form of the system while giving the extra degrees of freedom to enhance the controller performance. Instead of (2), the constructed dynamic equation in this study is given as

$$\dot{x}(t) = \big(A(\zeta) + \Delta A(x, \varsigma, \zeta, t)\big)x(t)$$
$$+B\big(u(t) + \psi(x, \varsigma, \zeta, u, t)\big) \qquad (3)$$

Choosing appropriate value of ζ with allowable range of the system operation, (3) can be written as

$$\dot{x}(t) = \big(A + \Delta A(x, \varsigma, t)\big)x(t)$$
$$+ B\big(u(t) + \psi(x, \varsigma, u, t)\big) \qquad (4)$$

where $A \in \mathbb{R}^{n \times n}$ is the system matrix, $B \in \mathbb{R}^{n \times m}$ is the input matrix and $\Delta A(x, \varsigma, t)$ and $\psi(x, \varsigma, u, t)$ are the norm bounded system uncertainty and the norm bounded input uncertainty, respectively.

(4) is a standard form as any nonlinear system and through extended linearization, matrix A and B can be chosen such that the pointwise controllability in the region of operation is maximized [10]. With the combination of deterministic approach, the norm bounded value of the uncertainties which affected by the value of ζ, can be chosen either small or large that suits a controller design criteria.

Based on (4), a nonlinear controller capable to be constructed. A multiobjective integral sliding mode control had constructed based on the following:
i)   The pair (A, B) is controllable.
ii) The state $x(t)$ is available.
iii) There exist continuous function $E(x, \varsigma, t) \in \mathbb{R}^{m \times n}$ and $H(x, \varsigma, t) \in \mathbb{R}^{m \times m}$ such that $\Delta A(x, \varsigma, t) = BE(x, \varsigma, t)$ and $\psi(x, \varsigma, u, t) = H(x, \varsigma, t)u(t)$ fulfill the matching condition.
iv) There exist known positive scalar-valued $\bar{E}, \bar{H}$ and $\bar{\psi}$ such that $\|E(x, \varsigma, t)\| \le \bar{E}$, $\|H(x, \varsigma, t)\| \le \bar{H}$ and $\|\psi(x, \varsigma, u, t)\| \le \bar{\psi}$.

The specifications and objectives of the designed controller include the following:
Ob1)   The control effort which maintain the sliding motion minimizes the following quadratic cost function

$$J = \int_0^\infty \big(x^T(t)Qx(t) + u(t)^T Ru(t)\big)\, dt \qquad (5)$$

for any initial state $x(0)$, where $Q = Q^T \in \mathbb{R}^{n \times n} \ge 0$ and $R = R^T \in \mathbb{R}^{m \times m} > 0$ are the weighting matrices.

Ob2)   All the poles of the system during sliding motion are required to lie in the LMI region $\mathcal{D}(\alpha, r, \vartheta)$ such that

$$\lambda_{eig}(A - BK) \subset \mathcal{D}(\alpha, r, \vartheta) \qquad (6)$$

where λ_{eig} is the eigenvalues of system $(A - BK)$ and $\mathcal{D}(\alpha, r, \vartheta)$ in the complex domain defined as:

$$\mathcal{D} = \{z \in \mathbb{C} : \text{Re}(z) < -\alpha, \text{Re}(z)^2 + \text{Im}(z)^2 < r^2, \text{Re}(z)\tan\vartheta < -|\text{Im}(z)|\} \tag{7}$$

In conclusion, multiobjective design allow for more flexible and accurate specification of the desirable closed-loop behavior. The most appropriate method to design a multiobjective controller is through linear matrix inequality (LMI). The following section will discuss the LMI representation for each of the required design objectives.

■3.0 MULTIOBJECTIVE INTEGRAL SLIDING MODE CONTROL

This section presents the key concepts of multiobjective integral sliding mode control proposed in this research. First, the stability analysis in the form of LMI for the closed-loop uncertain nonlinear system (4) was discussed. It followed by solving the optimization problem of the quadratic cost function (5) based on linear quadratic regulators (LQR) approach through LMI representation. Then, the pole placement problem will solved such that the closed-loop poles lie within a prescribed region in LMI form.

Based on some related studies had discussed in [15–17], the decision variables of the LMI constraints consist of the gain matrix K and the positive-definite symmetric matrix P. However, P matrix for decision variable involves is main focus in this study. To achieve this, it requires a proper selection of variables when constructing the LMI constraint. By reducing the number of decision variables, it will reduce the numerical burden at the cost of conservatism [18]. It results obtained may be efficient in practice.

The integral sliding surface and the stability analysis during sliding mode will discussed in next section.

3.1 Integral Sliding Surface and Stability Analysis

Define an integral sliding surface as

$$\sigma(t) = Gx(t) - G\int_0^t \left(Ax(\tau) + Bu_l(\tau)\right)d\tau \tag{8}$$

where $u_l(t) = -Kx(t)$ is a linear control term with $K = R^{-1}B^T P$ to be designed and $G \in \mathbb{R}^{m \times n}$ is the sliding surface parameter and is defined as $G = (B^T P^{-1}B)^{-1}B^T P^{-1}$. K is chosen such that matrix $(A - BK)$ is Hurwitz and G is chosen such that $GB = 1$ and its value dependent on $P \in R^{n \times n}$ where P a symmetric positive definite matrix.

According to the sliding mode control theory, as the state trajectory of system (4) reach the sliding surface, it follows that $\sigma(t) = 0$ and $\dot{\sigma}(t) = 0$ [20]. Therefore, by $\dot{\sigma}(t) = 0$, the equivalent control can be derived as

$$u_{eq}(t) = -Kx(t) - E(x, \varsigma, t)x(t) - \psi(x, \varsigma, u, t) \tag{9}$$

Substituting (9) into (4), the sliding dynamic can be obtained as

$$\dot{x}(t) = A_{cl}x(t) \tag{10}$$

where $A_{cl} = (A - BK)$. The system dynamics during sliding mode are independent of the system uncertainties and determined through proper selection of gain K. Gain K was calculated by

minimizing the cost function (5) and solving the pole placement problem located within LMI region (7).

Based on the sliding dynamics, the stability analysis is presented in the following theorem.

Theorem 1. *The sliding mode dynamic equation (10) is asymptotically stable, if there are matrix K and a symmetric matrix $\bar{P}_s > 0$ such that the following inequality is satisfied.*

$$A\bar{P}_s + \bar{P}_s A^T + BM + M^T B^T < 0 \tag{11}$$

Proof. Consider the following as the Lyapunov function candidate

$$V(t) = x^T(t)P_s x(t) \tag{12}$$

Calculating the time derivative of $V(t)$

$$\begin{aligned}\dot{V}(t) &= x^T(t)P_s\dot{x}(t) + \dot{x}^T(t)P_s x(t) \\ &= x^T(t)P_s\left(A_{cl}x(t)\right) + \left(A_{cl}x(t)\right)^T P_s x(t) \\ &= x^T(t)P_s Ax(t) + x^T(t)A^T P_s x(t) - x^T(t)P_s BKx(t) \\ &\quad - x^T(t)K^T B^T P_s x(t) \\ &= x^T(t)(P_s A + A^T P_s - P_s BR^{-1}B^T P_s \\ &\quad - P_s BR^{-1}B^T P_s)x(t)\end{aligned} \tag{13}$$

Define the following

$$M = -R^{-1}B^T \tag{14}$$

Thus, Equation (13) reduced becomes

$$\dot{V}(t) = x^T(t)(P_s A + A^T P_s + P_s BMP_s + P_s M^T B^T P_s)x(t) \tag{15}$$

Pre- and post-multiplying (15) with with $\bar{P}_s = P_s^{-1}$ and reduced becomes

$$\dot{V}(t) = x^T(t)(A\bar{P}_s + \bar{P}_s A^T + BM + M^T B^T)x(t) \tag{16}$$

Thus, if there exist matrix K such that the closed-loop system is Hurwitz and matrix $\bar{P}_s > 0$ that satisfies (11), the sliding mode dynamic Equation (10) is asymptotically stable.

The following section will discuss the LMI representation for Ob1) and Ob2).

3.2 Optimal Quadratic Performance

According to system presented in (4), the LQR problem is to determine the control $u(t)$ that minimizes the quadratic cost function (5). The solution relies on solving the algebraic Riccati equation (ARE)

$$A^T P_{op} + P_{op}A - P_{op}BR^{-1}B^T P_{op} + Q = 0 \tag{17}$$

and the minimum quadratic cost is given by

$$J_{min} = x(0)^T P_{op}x(0) \tag{18}$$

In the practice situation, (18) was reduced as

$$x(0)^T P_{op}x(0) \leq \varrho \tag{19}$$

where ϱ is the specified upper bound for the cost function, J. Hence, the above inequality can also be expressed as LMI:

$$\begin{bmatrix} \varrho & x(0)^T \\ x(0) & P_{op}^{-1} \end{bmatrix} \geq 0 \qquad (20)$$

By considering only the left hand side of (17) and in view of (14), the ARE can be solved as follows:

$$A^T P_{op} + P_{op} A - P_{op} B R^{-1} B^T P_{op} - P_{op} B R^{-1} B^T P_{op}$$
$$+ P_{op} B R^{-1} B^T P_{op} + Q$$
$$A^T P_{op} + P_{op} A - P_{op} B R^{-1} B^T P_{op} - P_{op} B R^{-1} B^T P_{op}$$
$$+ P_{op} B R^{-1} (R R^{-1}) B^T P_{op} + Q$$
$$A^T P_{op} + P_{op} A + P_{op} B M_{op} + P_{op} M^T B^T P_{op}$$
$$+ P_{op} M^T R M_{op} + Q \qquad (21)$$

Pre- and post-multiply (21) with $\bar{P}_{op} = P_{op}^{-1}$, leads to

$$\bar{P}_{op} A^T + A \bar{P}_{op} + B M + M^T B^T + M^T R M + \bar{P}_{op} Q \bar{P}_{op} \qquad (22)$$

Based on Cholesky factorization, the weighting matrices Q and R, can be deduced as $Q = \hat{Q}^T \hat{Q}$ and $R = \hat{R}^T \hat{R}$ with $\hat{Q}$ and $\hat{R}$ are the upper triangular with positive diagonal elements. Then, by utilizing the Schur complement, (22) can then be put into an inequality as follows:

$$\begin{bmatrix} \bar{P}_{op} A^T + A \bar{P}_{op} + B M + M^T B^T & \bar{P}_{op} \hat{Q}^T & M^T \hat{R}^T \\ \hat{Q} \bar{P}_{op} & -I_n & 0_{n \times m} \\ \hat{R} M & 0_{m \times n} & -I_m \end{bmatrix}$$
$$\leq 0 \qquad (23)$$

Thus, the LMI constraints that represent Ob1) are (20) and (23).

3.3 LMI Formulation for Pole Placement

In control systems design, fulfilling some desired transient performance objectives such as fast and well-damped transient response should be considered. For many practical problems, an accurate pole placement may not be necessary. It suffices to locate the closed-loop poles in a prescribed subregion in the complex left half plane. Thus, a Lyapunov characterisation of pole clustering region in terms of LMIs is discussed.

Definition 1 (LMI regions). [21] *A subset of $\mathcal{D}$ of the complex plane is called an LMI region if there exists a symmetric matrix $\gamma = [\gamma_{kl}] \in \mathbb{R}^{m \times m}$ and matrix $\beta = [\beta_{kl}] \in \mathbb{R}^{m \times m}$ such that*

$$\mathcal{D} = \{ z \in \mathbb{C} : \ f_{\mathcal{D}}(z) < 0 \} \qquad (24)$$

where

$$f_{\mathcal{D}}(z) := \gamma + z\beta + \bar{z}\beta^T$$
$$= [\gamma_{kl} + \beta_{kl} z + \beta_{lk} \bar{z}]_{1 \leq k, l \leq m} \qquad (25)$$

In this work, a region $\mathcal{D}(\alpha, r, \vartheta)$ as in (7) is chosen and is represented in Figure 1. The described region is a combination of α-stability, disks and conic sectors region.
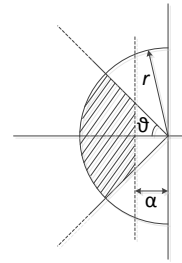

Figure 1 Region $\mathcal{D}(\alpha, r, \vartheta)$

By confining the closed-loop poles to this region it ensures a minimum decay rate α, a minimum damping ratio $\xi = \cos \vartheta$, and a maximum undamped natural frequency $\omega_d = r \sin \vartheta$. This in turn bounds the maximum overshoot, the frequency of oscillator modes, the delay time, the rise time, and the settling time.

The above region are said to be $\mathcal{D}$-stable for system (10) if the following theorem is fulfil

Theorem 2. [21] *A linear state space model $\dot{x}(t) = A_{cl} x(t)$ is $\mathcal{D}$-stable if and only if there exists a symmetric matrix $P_{re} > 0$ such that*

$$\gamma \otimes P_{re} + \beta \otimes (P_{re} A_{cl}) + \beta^T \otimes (P_{re} A_{cl})^T < 0 \qquad (26)$$

where the operator $\otimes$ is the so-called Kronecker product.

Proof. Refer to [21]

Based on Theorem 2, the chosen region (7) can be depicted by a set of three LMIs

$$2\alpha P_{re} + A^T P_{re} + P_{re} A - P_{re} B K - K^T B^T P_{re} < 0 \qquad (27)$$

$$\begin{pmatrix} \sin \vartheta \, (\Upsilon) & -\cos \vartheta \, (\Psi) \\ \cos \vartheta \, (\Psi) & \sin \vartheta \, (\Upsilon) \end{pmatrix} < 0 \qquad (28)$$

$$\begin{pmatrix} -r P_{re} & A^T P_{re} - K^T B^T P_{re} \\ P_{re} A - P_{re} B K & -r P_{re} \end{pmatrix} < 0 \qquad (29)$$

where $\quad \Upsilon = A^T P_{re} + P_{re} A - P_{re} B K - K^T B^T P_{re} \quad$ and $\quad \Psi = A^T P_{re} - P_{re} A + P_{re} B K - K^T B^T P_{re}$.

By pre- and post-multiplying (27)-(29) with $\bar{P}_{re} = P_{re}^{-1}$ and in view with (14), the LMIs can be rewritten as follows:

$$2\alpha \bar{P}_{re} + \bar{P}_{re} A^T + A \bar{P}_{re} + B M + M^T B^T < 0 \qquad (30)$$

$$\begin{pmatrix} \sin \vartheta \, (\bar{\Upsilon}) & -\cos \vartheta \, (\bar{\Psi}) \\ \cos \vartheta \, (\bar{\Psi}) & \sin \vartheta \, (\bar{\Upsilon}) \end{pmatrix} < 0 \qquad (31)$$

$$\begin{pmatrix} -r \bar{P}_{re} & \bar{P}_{re} A^T + M^T B^T \\ A \bar{P}_{re} + B M & -r \bar{P}_{re} \end{pmatrix} < 0 \qquad (32)$$

where $\quad \bar{\Upsilon} = \bar{P}_{re} A^T + A \bar{P}_{re} + B M + M^T B^T \quad$ and $\quad \bar{\Psi} = \bar{P}_{re} A^T - A \bar{P}_{re} + B M - M^T B^T$. Thus, the LMI constraints that represent Ob2) are as stated in (30)-(32).

3.4 Solution to Multiple Criteria Using Convex LMI

Solution to determine the multiobjective integral sliding mode control which minimized the control efforts in term of cost function (5), constraint closed-loop poles of the reduced order system in a robust LMI region (6) and the Lyapunov based stability analysis during the sliding motion (12), are represented as LMI sets (20) and (23), (30)-(32) and (11), respectively. The decision variables for these sets of LMIs are P_{op}, P_{re} and P_s are not directly related to produce a common solution. However, by letting $P_{op} = P_{re} = P_s = P$ and $\bar{P}_{op} = \bar{P}_{re} = \bar{P}_s = \bar{P}$ where $\bar{P} = P^{-1}$, a common solution for the LMIs set can be found. Thus, the LMIs set can be rewritten as the following

$$\begin{bmatrix} \varrho & x(0)^T \\ x(0) & \bar{P} \end{bmatrix} \geq 0 \tag{33}$$

$$\begin{bmatrix} \bar{P}A^T + A\bar{P} + BM + M^TB^T & \bar{P}\hat{Q}^T & M^T\hat{R}^T \\ \hat{Q}\bar{P} & -I_n & 0_{n\times m} \\ \hat{R}M & 0_{m\times n} & -I_m \end{bmatrix} \leq 0 \tag{34}$$

$$2\alpha\bar{P} + \bar{P}A^T + A\bar{P} + BM + M^TB^T < 0 \tag{35}$$

$$\begin{pmatrix} \sin\vartheta\,(\bar{Y}^*) & -\cos\vartheta\,(\bar{\Psi}^*) \\ \cos\vartheta\,(\bar{\Psi}^*) & \sin\vartheta\,(\bar{Y}^*) \end{pmatrix} < 0 \tag{36}$$

$$\begin{pmatrix} -r\bar{P} & \bar{P}A^T + M^TB^T \\ A\bar{P} + BM & -r\bar{P} \end{pmatrix} < 0 \tag{37}$$

$$A\bar{P} + \bar{P}A^T + BM + M^TB^T < 0 \tag{38}$$

$$\bar{P} > 0 \tag{39}$$

where $\bar{Y}^* = \bar{P}A^T + A\bar{P} + BM + M^TB^T$ and $\bar{\Psi}^* = \bar{P}A^T - A\bar{P} + BM - M^TB^T$.

■4.0 INTEGRAL SLIDING MODE CONTROLLER AND REACHABILITY ANALYSIS

In this study, the reaching control law is selected as

$$u(t) = u_l(t) + u_{nl}(t) \tag{40}$$

where the linear part of the controller is responsible for the nominal performance of the system. It is given as

$$u_l(t) = -Kx(t) \tag{41}$$

while the nonlinear part is responsible for compensating the system uncertainties and it is given as

$$u_{nl}(t) = -\big(\varphi + \rho(t)\big)\text{sign}\big(\sigma(t)\big) \tag{42}$$

where $\rho(t) = \bar{E}\|x(t)\| + \bar{\psi}$ and $\varphi > 0$ is a design parameter.

Theorem 3. *Consider an uncertain system (4), the reaching condition $\sigma(t)\dot{\sigma}(t) < 0$ is satisfied by employing the control law $u(t)$ given below:*

$$u(t) = -Kx(t) - \big(\varphi + \rho(t)\big)\text{sign}\big(\sigma(t)\big) \tag{43}$$

where $\varphi > 0$, $\rho(t) = \bar{E}\|x(t)\| + \bar{\psi}$ and gain K is chosen such that A_{cl} is Hurwitz, then the trajectory of the uncertain system (4) is forced to move from any initial condition to the sliding surface $\sigma(t) = 0$ in finite time and to remain on it.

Proof. Consider the following as the Lyapunov function candidate

$$V(t) = \frac{1}{2}\sigma^2(t) \tag{44}$$

Calculating the time derivative of $V(t)$

$$\begin{aligned} \dot{V}(t) &= \sigma(t)\dot{\sigma}(t) \\ &= \sigma(t)\big(u(t) + Kx(t) + E(x,\varsigma,t)x(t) + \psi(x,\varsigma,u,t)\big) \\ &= \sigma(t)\Big(-Kx(t) - \big(\varphi + \rho(t)\big)\text{sign}\big(\sigma(t)\big) + Kx(t) \\ &\qquad\qquad + E(x,\varsigma,t)x(t) + \psi(x,\varsigma,u,t)\Big) \\ &= -\sigma(t)\varphi\,\text{sign}\big(\sigma(t)\big) - \sigma(t)\bar{E}\|x(t)\|\,\text{sign}\big(\sigma(t)\big) \\ &\qquad\qquad - \sigma(t)\bar{\psi}\,\text{sign}\big(\sigma(t)\big) + \sigma(t)E(x,\varsigma,t)x(t) \\ &\qquad\qquad + \sigma(t)\psi(x,\varsigma,u,t) \\ &= -\varphi\|\sigma(t)\| - \bar{E}\|x(t)\|\|\sigma(t)\| - \bar{\psi}\|\sigma(t)\| + \sigma(t)E(x,\varsigma,t)x(t) \\ &\qquad\qquad + \sigma(t)\psi(x,\varsigma,u,t) \\ &\leq -\varphi\|\sigma(t)\| - \bar{E}\|x(t)\|\|\sigma(t)\| - \bar{\psi}\|\sigma(t)\| \\ &\qquad\qquad + \|E(x,\varsigma,t)\|\|x(t)\|\|\sigma(t)\| \\ &\qquad\qquad + \|\psi(x,\varsigma,u,t)\|\|\sigma(t)\| \\ &\leq -\varphi\|\sigma(t)\| - \bar{E}\|x(t)\|\|\sigma(t)\| - \bar{\psi}\|\sigma(t)\| + \bar{E}\|x(t)\|\|\sigma(t)\| \\ &\qquad\qquad + \bar{\psi}\|\sigma(t)\| \\ &\leq -\varphi\|\sigma(t)\| \end{aligned} \tag{45}$$

Based on the Lyapunov theory, as $\dot{V}(t) = -\varphi\|\sigma(t)\| < 0$ for any $\sigma(t) \neq 0$ the trajectory of the system are driven onto the sliding surface $\sigma(t) = 0$ and maintained there for all subsequent time. Thus, the proof is complete.

It is well known that the discontinuous switching function $\text{sign}\big(\sigma(t)\big)$ as in (43) will cause chattering of the control signals [22]. This chattering may bring damage to the actuator or excite high-frequency unmodelled dynamics in the system which causes system instability. To avoid such unwanted conditions, the discontinuous function is approximated by a continuous/smooth function. Thus, a sigmoid function is chosen

$$\text{sign}\big(\sigma(t)\big) \approx \frac{\sigma(t)}{|\sigma(t)| + \delta} \tag{46}$$

where δ is a small positive scalar value. Aside from avoiding (40) from going into infinite value each time sliding surface is reached, the value of δ should be selected as tradeoff between the accuracy of the system performance and smooth control action. Using this function, the controller (43) becomes

$$u(t) = -Kx(t) - \big(\varphi + \rho(t)\big)\frac{\sigma(t)}{|\sigma(t)| + \delta} \tag{47}$$

■5.0 APPLICATION TO THE ROTARY INVERTED PENDULUM SYSTEM

Rotary inverted pendulum system is composed of a pendulum, rotating arm, motor and encoders. The system is inherently nonlinear, under-actuated, non-minimum phase and unstable. In this control system, the arm is revolved to stabilize the pendulum at its upright position. The overview of the system is presented in Figure 2.
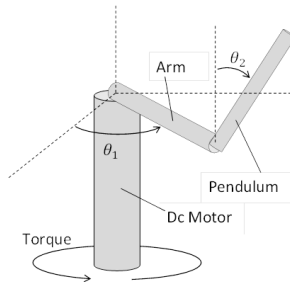
Figure 2 Rotary inverted pendulum system

Under no load condition, the following nonlinear motion equations of the rotary inverted pendulum system are those of Euler-Lagrange are as given in [3]:

$$\begin{aligned}
&\left(J_1 + m_2 l_1^2 + m_2 c_2^2 \sin^2\big(\theta_2(t)\big)\right)\ddot{\theta}_1(t)\\
&\qquad\qquad +m_2 l_1 c_2 \cos\big(\theta_2(t)\big)\ddot{\theta}_2(t) -\\
&m_2 l_1 c_2 \sin\big(\theta_2(t)\big)\dot{\theta}_2^2(t)\\
&\quad +m_2 c_2^2 \dot{\theta}_1(t)\dot{\theta}_2(t)\sin\big(2\theta_2(t)\big) = \tau_m(t)
\end{aligned} \tag{48}$$

$$\begin{aligned}
&\big(m_2 l_1 c_2 \cos\big(\theta_2(t)\big)\big)\ddot{\theta}_1(t) + \big(J_2 + m_2 c_2^2\big)\ddot{\theta}_2(t)\\
&\quad +\left(-\tfrac{1}{2}m_2 c_2^2 \dot{\theta}_1(t)\sin\big(2\theta_2(t)\big)\right)\dot{\theta}_1(t)\\
&\quad -m_2 g c_2 \sin\big(\theta_2(t)\big) = 0
\end{aligned} \tag{49}$$

where $\tau_m(t) = \frac{K_t}{R_m}u(t) - \frac{K_t K_b}{R_m}\dot{\theta}_1(t)$ is the torque applied to the arm of the system with $u(t)$ is a voltage supplied to the actuator. The values of the parameters of the system are summarized in Table 1.

Under the influence of load mounted at the free end of the pendulum, the value of the center of mass, c_2 and the inertia of the pendulum, J_2 will be affected [23]. Figure 3 shows the hollow cylinder load attached to the pendulum with parameters tabulated in Table 2.

Table 1 Parameters of the rotary inverted pendulum system

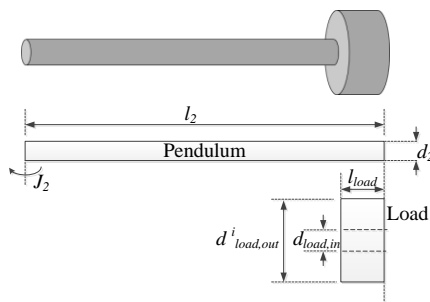| Symbol	Description	Value
m_1	Mass of arm (kg)	0.056
m_2	Mass of pendulum (kg)	0.022
l_1	Length of arm (m)	0.16
l_2	Length of pendulum (m)	0.16
c_1	Distance to the center of mass of arm (m)	0.08
c_2	Distance to the center of mass of pendulum (m)	0.08 (no load)
d_2	Diameter of pendulum (m)	0.008
g	Gravitational constant (m/s^2)	9.8
J_1	Inertia of arm (kgm^2)	0.00215058
J_2	Inertia of pendulum (kgm^2)	0.00018773 (no load)
R_m	Armature resistance (Ω)	2.5604
K_b	Back-emf constant (Vs/rad)	0.01826
K_t	Torque constant (Nm/A)	0.01826

Figure 3 Pendulum with attached load

Table 2 Parameters of load configuration

Symbol	Description	Value			
l_{load}	Length of load (m)	0.0049			
$d_{load,in}$	Diameter of hollow portion (m)	0.004			
m_{load}^i	Mass of load (kg)	0.005	0.010	0.015	0.020
$d_{load,out}^i$	Diameter of load (m)	0.01	0.016	0.019	0.0232

*where $i = 1, 2, \dots, 4$ indicates the various load weight and its corresponding diameter.

Based on the load configuration, the center of mass and inertia of pendulum can be calculated as the following:

$$c_2 = \frac{m_2 \frac{l_2}{2} + m_{load}^i \left(l_2 - \frac{l_{load}}{2}\right)}{m_2 + m_{load}^i} \tag{50}$$

$$\begin{aligned}
J_2 &= \left(\frac{1}{12}m_2\left(3\left(\frac{d_2}{2}\right)^2 + l_2^2\right) + m_2\left(\frac{l_2}{2}\right)^2\right)\\
&+ \left(\begin{aligned}&\frac{1}{12}m_{load}^i\left[3\left(\frac{\left(d_{load,out}^i\right)^2}{2} + \frac{d_{load,in}^2}{2}\right) + l_{load}^2\right]\\&+ m_{load}^i\left(l_2 - \frac{l_{load}}{2}\right)^2\end{aligned}\right)
\end{aligned} \tag{51}$$

By considering the effect of load towards the rotary inverted pendulum systems, the motion equations of (48) and (49) becomes

$$\begin{aligned}
&\left(\begin{aligned}&J_1 + \big(m_2 + m_{load}^i\big)l_1^2\\&+\big(m_2 + m_{load}^i\big)c_2^2 \sin^2\big(\theta_2(t)\big)\end{aligned}\right)\ddot{\theta}_1(t)\\
&\quad +\big(m_2 + m_{load}^i\big)l_1 c_2 \cos\big(\theta_2(t)\big)\ddot{\theta}_2(t)\\
&\quad -\big(m_2 + m_{load}^i\big)l_1 c_2 \sin\big(\theta_2(t)\big)\dot{\theta}_2^2(t)\\
&\quad +\big(m_2 + m_{load}^i\big)c_2^2 \dot{\theta}_1(t)\dot{\theta}_2(t)\sin\big(2\theta_2(t)\big) = \tau_m(t)
\end{aligned} \tag{52}$$

$$\begin{aligned}
&\left(\big(m_2 + m_{load}^i\big)l_1 c_2 \cos\big(\theta_2(t)\big)\right)\ddot{\theta}_1(t)\\
&\quad +\big(J_2 + \big(m_2 + m_{load}^i\big)c_2^2\big)\ddot{\theta}_2(t)\\
&\quad +\left(-\tfrac{1}{2}\big(m_2 + m_{load}^i\big)c_2^2 \dot{\theta}_1(t)\sin\big(2\theta_2(t)\big)\right)\dot{\theta}_1(t)\\
&\quad -\big(m_2 + m_{load}^i\big)g c_2 \sin\big(\theta_2(t)\big) = 0
\end{aligned} \tag{53}$$

For the sake of simplicity, the time variables is omitted, thus (52) and (53) can be rearranged as follows

$$\begin{aligned}
\ddot{\theta}_1 &= \frac{1}{\varepsilon}P_4 P_6 \dot{\theta}_1 + \frac{1}{\varepsilon}P_2 P_3 \sin(\theta_2)\cos^2(\theta_2)\dot{\theta}_1^2\\
&\quad -\frac{1}{\varepsilon}P_3 P_4 \sin(\theta_2)\dot{\theta}_2^2\\
&\quad +\frac{1}{\varepsilon}2P_2 P_4 \sin(\theta_2)\cos(\theta_2)\dot{\theta}_1\dot{\theta}_2\\
&\quad +\frac{1}{\varepsilon}P_3 P_5 \sin(\theta_2)\cos(\theta_2) - \frac{1}{\varepsilon}P_4 P_7 u
\end{aligned} \tag{54}$$

$$\begin{aligned}
\ddot{\theta}_2 &= -\frac{1}{\varepsilon}P_3 P_6 \cos(\theta_2)\dot{\theta}_1\\
&\quad -\frac{1}{\varepsilon}\big(P_2(P_1 + P_2 \sin^2(\theta_2))\sin(\theta_2)\cos(\theta_2)\big)\dot{\theta}_1^2\\
&\quad +\frac{1}{\varepsilon}P_3^2 \sin(\theta_2)\cos(\theta_2)\dot{\theta}_2^2\\
&\quad -\frac{1}{\varepsilon}2P_2 P_3 \sin(\theta_2)\cos^2(\theta_2)\dot{\theta}_1\dot{\theta}_2\\
&\quad -\frac{1}{\varepsilon}P_5(P_1 + P_2 \sin^2(\theta_2))\sin(\theta_2)
\end{aligned} \tag{55}$$

$$+\frac{1}{\varepsilon}P_3 P_7 \cos(\theta_2)\, u$$

where

$$P_1 = J_1 + \left(m_2 + m_{load}^i\right)l_1^2\,, \quad P_2 = \left(m_2 + m_{load}^i\right)c_2^2$$
$$P_3 = \left(m_2 + m_{load}^i\right)l_1 c_2\,, \quad P_4 = \left(J_2 + \left(m_2 + m_{load}^i\right)c_2^2\right)$$
$$P_5 = \left(m_2 + m_{load}^i\right)g c_2\,, \quad P_6 = \frac{K_t K_b}{R_m}\,, \quad P_7 = \frac{K_t}{R_m}$$
$$\varepsilon = P_3^2 \cos^2(\theta_2) - P_1 P_4 - P_2 P_4 \sin^2(\theta_2)$$

By defining the state variables as $[x_1(t), x_2(t), x_3(t), x_4(t)]^T = \left[\theta_1(t), \dot{\theta}_1(t), \theta_2(t), \dot{\theta}_2(t)\right]^T$, (54) and (55) can be written as the following form

$$\dot{x}(t) = \left(A + \Delta A\left(x, m_{load}^i, d_{load,out}^i, t\right)\right)x(t)$$
$$+ B\left(u(t) + \psi\left(x, m_{load}^i, d_{load,out}^i, u, t\right)\right) \quad (56)$$

where $A \in \mathbb{R}^{n \times n}$ is the system matrix, $B \in \mathbb{R}^{n \times m}$ is the input matrix, $x(t) \in \mathbb{R}^n$ is the system state, $u(t) \in \mathbb{R}^m$ is the control input while $\Delta A\left(x, m_{load}^i, d_{load,out}^i, t\right)$ and $\Delta B\left(x, m_{load}^i, d_{load,out}^i, u, t\right)$ are the system matrix uncertainty and input matrix uncertainty, respectively that cause by the load variation.

It is assumed that the allowable ranges of the system operations are

-2π rad $\le x_1 \le 2\pi$ rad
-628.3 rad/s $\le x_2 \le 628.3$ rad/s
$-1/4\pi$ rad $\le x_3 \le 1/4\pi$ rad
-20.3 rad/s $\le x_4 \le 20.3$ rad/s

Thus, by using both the extended linearization method and deterministic approach and the parameters as in Table 1 and Table 2, the following values are obtained [14]

$$A = \begin{bmatrix} 0 & 1 & 0 & 0 \\ 0 & -0.0646 & 48.2066 & 0 \\ 0 & 0 & 0 & 1 \\ 0 & -0.0585 & 14.4382 & 0 \end{bmatrix}, \quad B = \begin{bmatrix} 0 \\ 2.5333 \\ 0 \\ -1.7164 \end{bmatrix}$$
$$\bar{E} = 21.5353\,, \quad \bar{H} = 0.0434\,, \quad \bar{\psi} = 0.8683$$

Next section will discuss the simulation results between the multiobjective ISMC, normal ISMC and LQR.

■6.0 SIMULATION RESULTS AND DISCUSSION

In this section, simulation work is conducted to show the effectiveness of the proposed design method of the multiobjective ISMC. The design is based on the LMI algorithms that fulfilled both of the design objectives Ob1) and Ob2) and the closed-loop stability analysis of system (4). The simulation is performed by using MATLAB/Simulink while the LMI problem is solved by using Yalmip/SeDuMi toolbox. The performance of the proposed controller is compared with an LQR and a normal ISMC which the design is solely based on the stability of the system (11). This simulation will show the advantages of implementing multiobjective in controller design.

In rotary inverted pendulum system, there are tradeoff between the system performance and the control input supplied by the controller. For faster response, the system requires much higher control input. This is due to the torque needed by the arm to push the pendulum faster towards the vertical position. An

example can be shown in Figure 4. The results indicate that, higher control signal is needed to revolve the arm faster in order to quickly stabilize the pendulum. However, this cause the pendulum to overshoot up to -7° before stabilizes at the upright position. Even though the pendulum can be stabilized in less than 2 seconds, it is however not practical to let the controller produce such high signal since there is an input limitation of an actuator.

For the second scenario, if lower control input is designed, the pendulum will take nearly 5 seconds to reach the vertical position as shown in Figure 5. The results indicate that, lower control input signal is applied to the actuator which caused the arm to revolve slower since the torque generated is lower. As a result, the arm took much wider angle compared to the first scenario when balancing the pendulum. Note that, if the torque supplied by the actuator is too small, the arm might not be able to push the pendulum upwards and balance it. Thus, higher control signal which sometime larger than the operating range of the actuator might be needed to produce enough torque such that the arm is able to push and later balance the pendulum in the upright position.


a)

b)
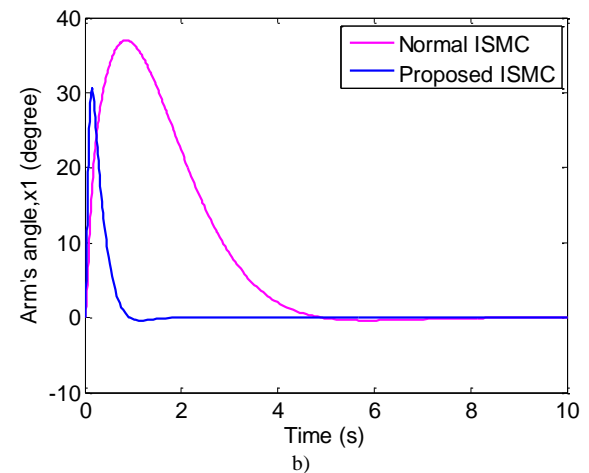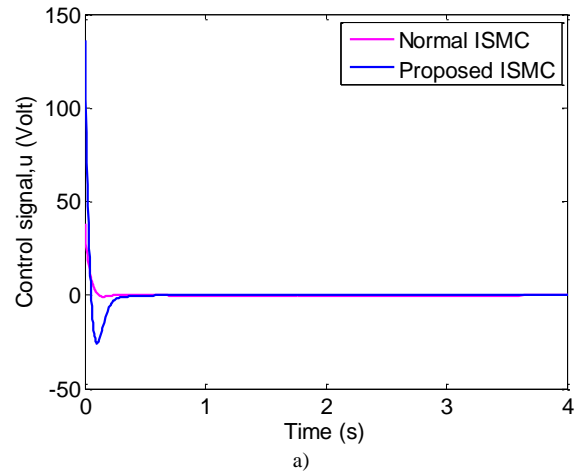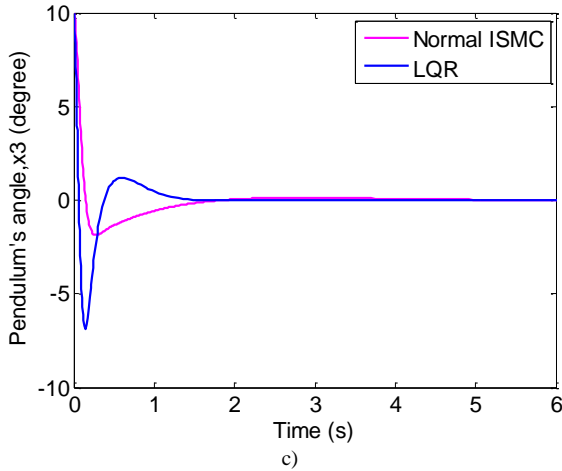
Figure 4 Simulation results of multiobjective integral sliding mode controller and normal integral sliding mode controller for fast response design, a) control input, b) arm's angle and c) pendulum's angle
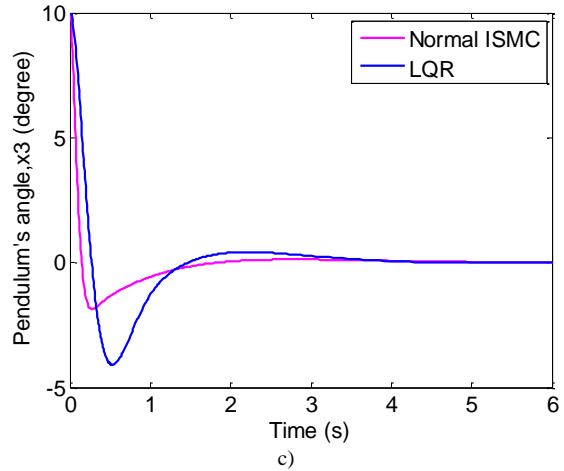
Figure 5 Simulation results of multiobjective integral sliding mode controller and normal integral sliding mode controller for slow response design, a) control input, b) arm's angle and c) pendulum's angle
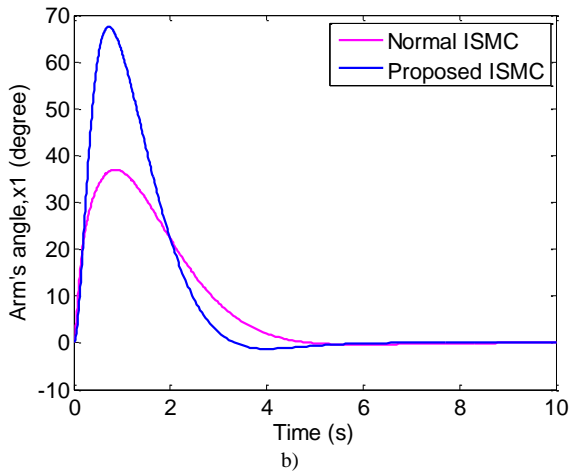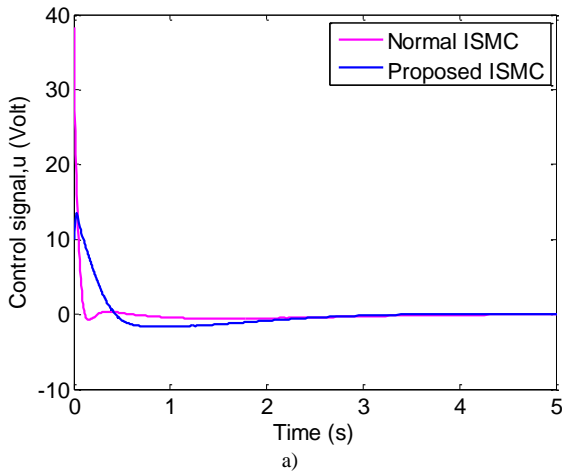
Next, the performance of the proposed controller is compared with a normal ISMC which the design is based on stability only and an LQR. The effect of varying load is also considered in the system performance. The performance of each controller had evaluated based on the integral of absolute-value error (IAE) where the regulator problem is treated as a special case of tracking control problem with the desired trajectories are considered zero. The IAE is calculated based on the following formula:

$$IAE = \int_0^T |x_i(t) - x_{i,d}(t)| dt \qquad (57)$$

where $x_i(t)$ (where $i = 1,2,...,n$) is the system state trajectory and $x_{i,d}(t)$ is the desired state trajectory which is assumed to be zero for regulator problem. The upper limit T is a finite time chosen somewhat arbitrarily so that the integral approaches a steady-state value.

In this simulation, it is assumed that the maximum control input that can be supplied to the actuator is 20Volts. In order to avoid saturation of the control input and at the same time fast system response, the following parameters are chosen:

$$Q = \begin{bmatrix} 10 & 0 & 0 & 0 \\ 0 & 1 & 0 & 0 \\ 0 & 0 & 5 & 0 \\ 0 & 0 & 0 & 1 \end{bmatrix}, \quad R = 1000, \quad \begin{array}{l} x(0) \\ = [0,0,0,0]^T \end{array}$$

$$\varrho = 480, \qquad \alpha = 2.4, \qquad r = 12$$
$$\vartheta = 60°, \qquad \varphi = 1.5, \qquad \delta = 0.1$$

Based on the LMI constraints (33)-(39), the symmetric positive definite matrix P is calculated as

$$P = \begin{bmatrix} 0.068 & 0.039 & 0.621 & 0.090 \\ 0.039 & 0.025 & 0.424 & 0.061 \\ 0.621 & 0.424 & 8.014 & 1.204 \\ 0.090 & 0.061 & 1.204 & 0.187 \end{bmatrix} \times 10^5$$

From here, the gain matrix K that affect the performance of the system is given as

$$K = R^{-1}B^T P = [-5.51 \quad -4.15 \quad -98.38 \quad -16.67]$$

while the close-loop poles are located at -5.67±j5.05, -3.90 and -2.93. Thus, by implementing controller (47) to system (56) under no load condition (Figure 6–Figure 7) and under various load condition (Figure 8–Figure 9) the following responses are obtained.


a)

b)

c)

d)

e)
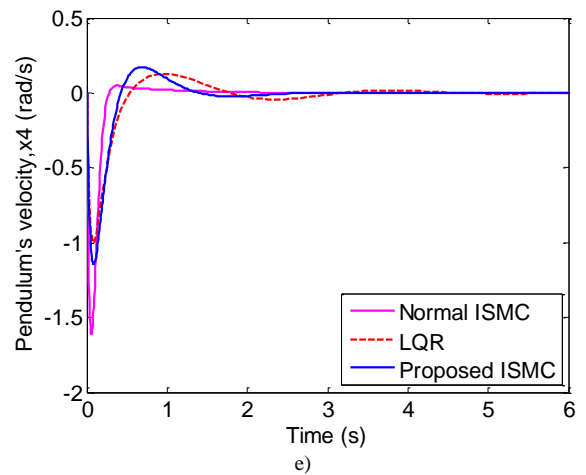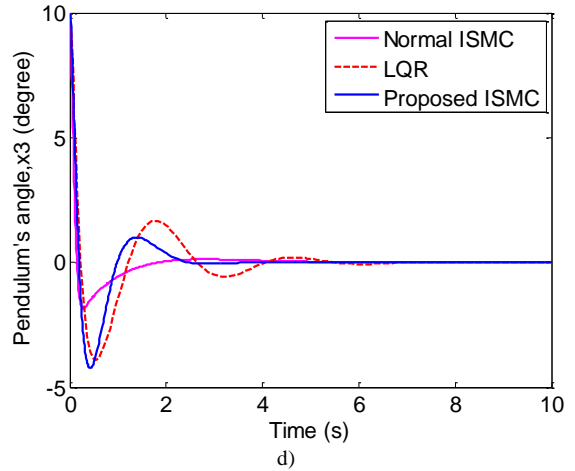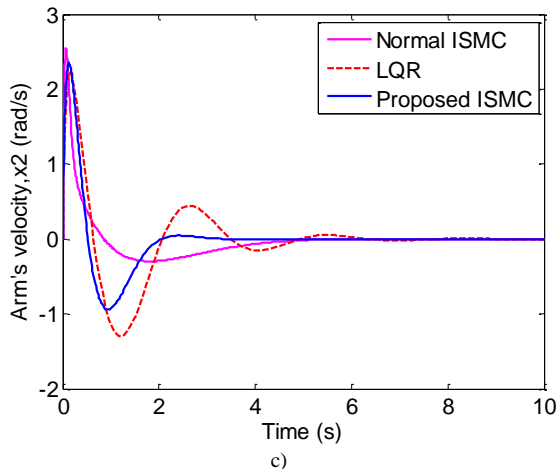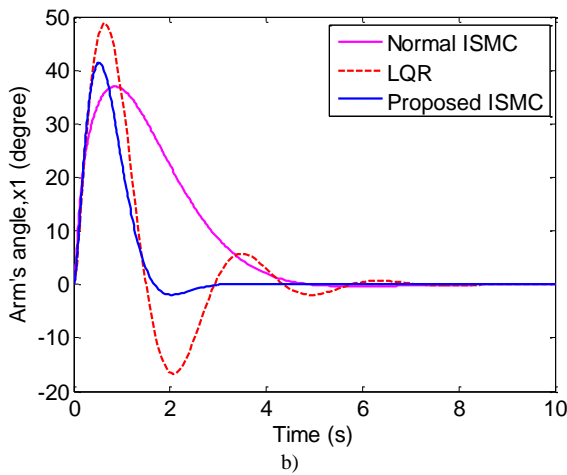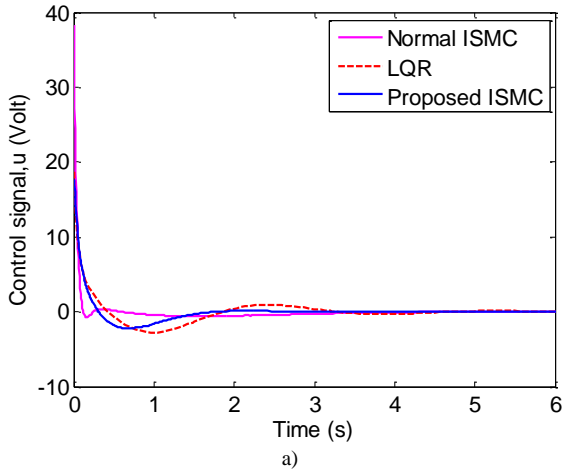
Figure 6 Simulation results of multiobjective ISMC, normal ISMC and LQR under no load condition with initial conditions $x(0) = [0 , 0 , 10° , 0]^T$, a) control input, b) arm's angle, c) arm's velocity, d) pendulum's angle and e) pendulum's velocity

a)
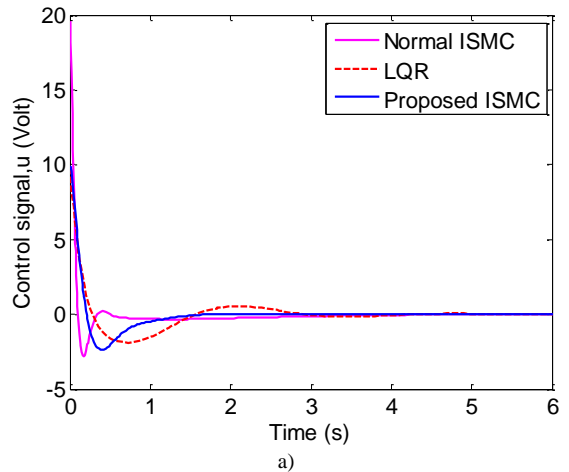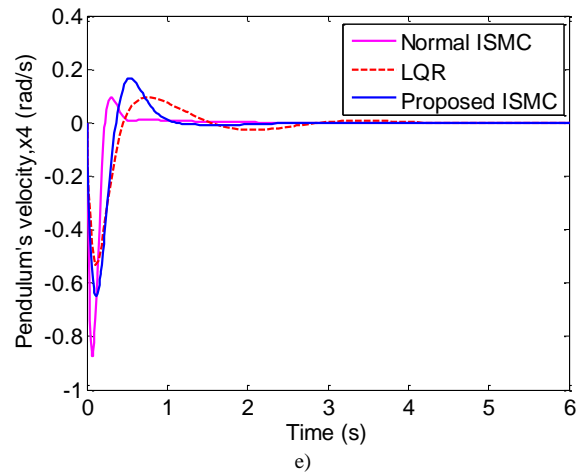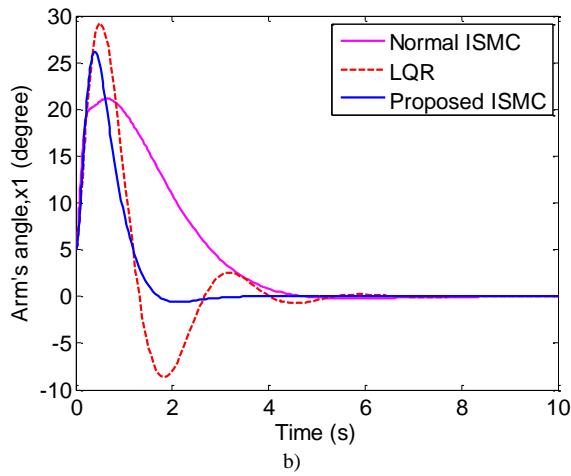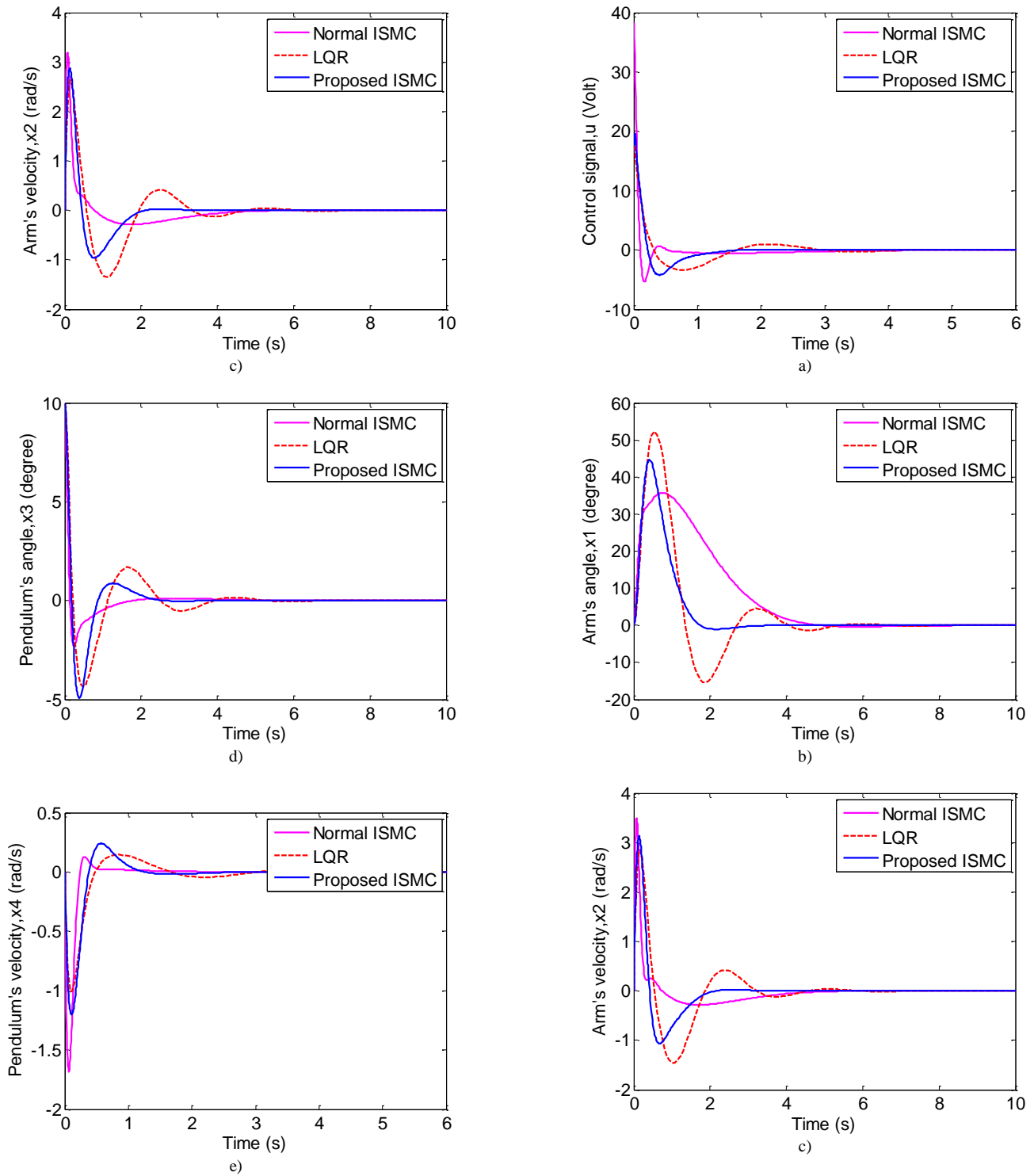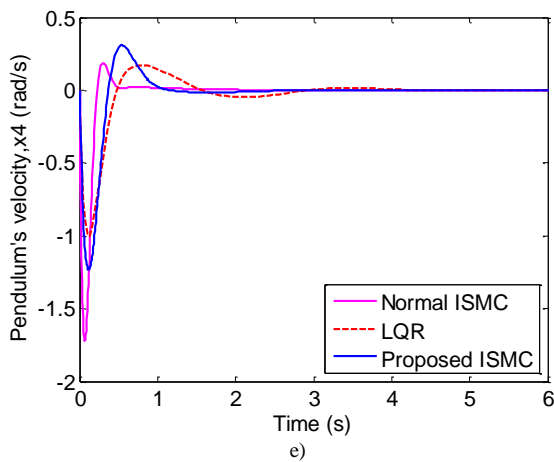
Figure 7 Simulation results of multiobjective ISMC, normal ISMC and LQR under no load condition with initial conditions $x(0) = [5°, 0, 5°, 0]^T$, a) control input, b) arm's angle, c) arm's velocity, d) pendulum's angle and e) pendulum's velocity
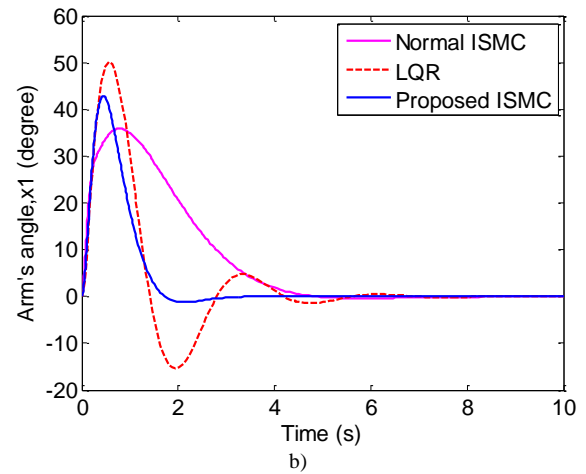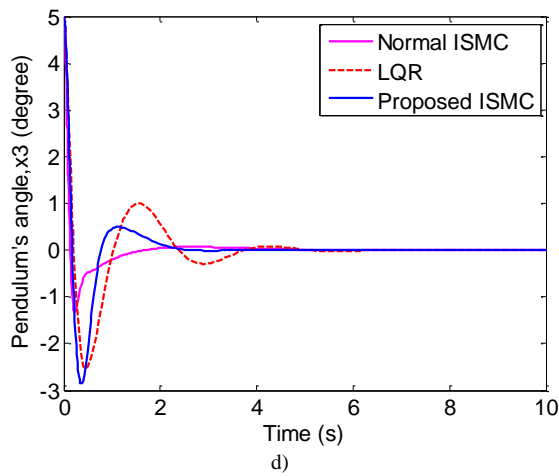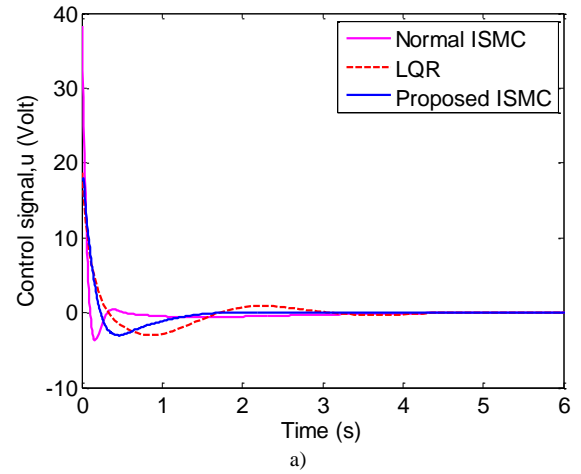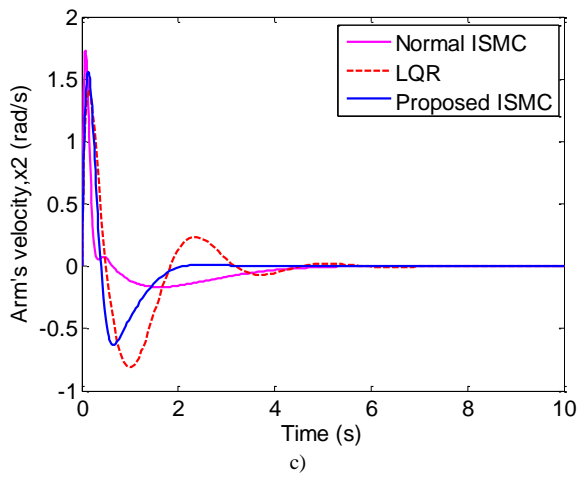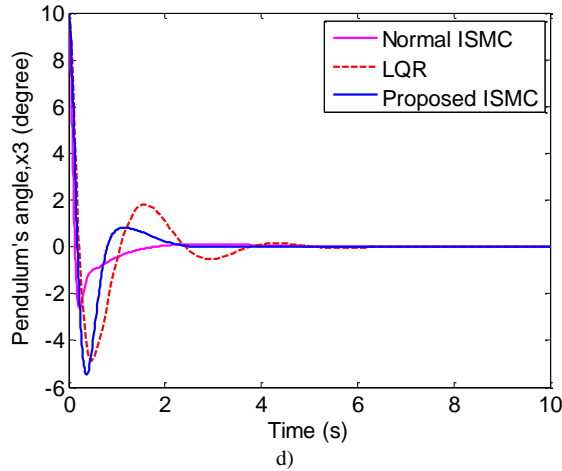
Figure 8 Simulation results of multiobjective ISMC, normal ISMC and LQR for 10g load, a) control input, b) arm's angle, c) arm's velocity, d) pendulum's angle and e) pendulum's velocity

d)

e)

Figure 9 Simulation results of multiobjective ISMC, normal ISMC and LQR for 20g load, a) control input, b) arm's angle, c) arm's velocity, d) pendulum's angle and e) pendulum's velocity

Figure 6–Figure 9 show the response of the normal ISMC, LQR and the multiobjectives ISMC when no load, 10 g and 20 g of load are applied to the system, respectively. The figures show the control signal generated by the respective controller, the trajectory of the arm and the trajectory of the pendulum during balancing. The performance of each controller is depicted as IAE performance index in Table 3–Table 6 for comparison purposes.

Table 3 IAE values and maximum generated control signal using normal ISMC, LQR and multiobjective ISMC under no load condition with initial conditions $x(0) = [0, 0, 10°, 0]^T$

Method	$u(t)$ (V)	IAE			
		$x_1(t)$	$x_2(t)$	$x_3(t)$	$x_4(t)$
Normal ISMC	38.25	1.4000	1.304	0.0382	0.2437
LQR	18.69	1.1530	2.5890	0.1005	0.4001
Proposed ISMC	17.74	0.6475	1.5170	0.0665	0.3597

Table 4 IAE values and maximum generated control signal using normal ISMC, LQR and multiobjective ISMC under no load condition with initial conditions $x(0) = [5°, 0, 5°, 0]^T$

Method	$u(t)$ (V)	IAE			
		$x_1(t)$	$x_2(t)$	$x_3(t)$	$x_4(t)$
Normal ISMC	19.56	0.7728	0.6586	0.01837	0.1364
LQR	9.78	0.5819	1.3580	0.0524	0.2258
Proposed ISMC	9.80	0.3583	0.8462	0.0336	0.2045

Table 5 IAE values and maximum generated control signal using normal ISMC, LQR and multiobjective ISMC under 10g of load

Method	$u(t)$ (V)	IAE			
		$x_1(t)$	$x_2(t)$	$x_3(t)$	$x_4(t)$
Normal ISMC	38.25	1.3530	1.2640	0.03681	0.2589
LQR	18.69	1.0630	2.5320	0.09827	0.4124
Proposed ISMC	18.03	0.6124	1.5410	0.06435	0.3787

Table 6 IAE values and maximum generated control signal using normal ISMC, LQR and multiobjective ISMC under 20g of load

Method	$u(t)$ (V)	IAE			
		$x_1(t)$	$x_2(t)$	$x_3(t)$	$x_4(t)$
Normal ISMC	38.25	1.3430	1.2600	0.03655	0.2698
LQR	18.69	1.0340	2.5880	0.10080	0.4332
Proposed ISMC	19.54	0.6015	1.5970	0.06455	0.3946

Based on the simulated responses and the calculated performance index, the trajectory of the pendulum's angle for the normal ISMC design based on the stability only, reach the upright position faster compare to the other two controllers. However, the arm takes much longer time to reach the steady state. Notice also, the control signal generated by the controller is larger than the acceptable range of the actuator which could cause the input signal to saturate.

The LQR performance is within the acceptable range of the system. The control signal generated is within the actuator's operating range but the performance is much slower. The proposed controller performs better than the LQR in both transient response and IAE performance and also generally better than the normal ISMC in terms of control signal and the arm's trajectory. However, pendulum's angle response, the proposed controller response is almost similar to the normal ISMC but with larger IAE performance.

Based on these results, the proposed controller able to perform faster, better transient response and lower control signal due to the design flexibility given by implementing Ob1) and Ob2) through LMI.

■7.0 CONCLUSION

This work offered an LMI-based multiobjective integral sliding mode controller to improve the performance of a continuous-time uncertain nonlinear system under various load condition. The proposed method able to obtain fast transient response and operated within the allowable operating range of the actuator even under the influence of varying load. Simulation results illustrate that the proposed control method offers better performance for uncertain nonlinear system.

References

[1] Furuta, K., M. Yamakita, and S. Kobayashi. 1992. Swing-up Control of Inverted Pendulum Using Pseudo-state Feedback. Proceedings of the Institution of Mechanical Engineers, Part I. *Journal of Systems and Control Engineering*. 206(4): 263–269.
[2] Cazzolato, B. S., and Z. Prime. 2011. On the Dynamics of the Furuta Pendulum. *Journal of Control Science and Engineering*. 2011: 8.

[3]   Fantoni, I., and R. Lozano. 2002. Stabilization of the Furuta Pendulum Around Its Homoclinic Orbit. *International Journal of Control*. 75(6): 390–398.

[4]   Park, M. S., and D. Chwa. 2009. Swing-Up and Stabilization Control of Inverted-Pendulum Systems via Coupled Sliding-Mode Control Method. *IEEE Transactions on Industrial Electronics*. 56(9): 3541–3555.

[5]   Hassanzadeh, I., and S. Mobayen. 2011. Controller Design for Rotary Inverted Pendulum System Using Evolutionary Algorithms. *Mathematical Problems in Engineering*.

[6]   Muske, K. R., H. Ashrafiuon, S. Nersesov, and M. Nikkhah. 2012. Optimal Sliding Mode Cascade Control for Stabilization of Underactuated Nonlinear Systems. *Journal of Dynamic Systems, Measurement, and Control*. 134(2): 21020–21030.

[7]   Friedland, B. 1995. *Advanced Control System Design*. New Jersey: Prentice-Hall, Inc.

[8]   Wernli, A., and G. Cook. 1975. Suboptimal Control for the Nonlinear Quadratic Regulator Problem. *Automatica*. 11(1): 75–84.

[9]   Mracek, C. P., and J. R. Cloutier. 1998. Control Designs for the Nonlinear Benchmark Problem via the State-dependent Riccati Equation Method. International *Journal of Robust and Nonlinear Control*. 8(4–5): 401–433.

[10] Çimen, T. 2010. Systematic and Effective Design of Nonlinear Feedback Controllers via the State-Dependent Riccati Equation (SDRE) method. *Annual Reviews in Control*. 34(1): 32–51.

[11] Yang, W., N. Hammoudi, G. Herrmann, M. Lowenberg, and X. Chen. 2015. Dynamic Gain-scheduled Control and Extended Linearisation: Extensions, Explicit Formulae and Stability. *International Journal of Control*. 88(1): 163–179.

[12] Lee, T. S. 2003. Nonlinear State Feedback Control Design for Three-phase PWM Boost Rectifiers Using Extended Linearisation. *IEE Proceedings of Electric Power Applications*. 150(5): 546–554.

[13] Wang, J., and N. Sundararajan. 1996. Extended Nonlinear Flight Controller Design for Aircraft. *Automatica*. 32(8): 1187–1193.

[14] Osman, J. H. S., and P. D. Roberts. 1995. A Two-level Control Strategy for Robot Manipulators. *International Journal of Control*. 61(6): 1201–1222.

[15] Olalla, C., R. Leyva, A. El-Aroudi, and I. Queinnec. 2009. Robust LQR Control for PWM Converters: An LMI Approach. *IEEE Transactions on Industrial Electronics*. 56(7): 2548–2558.

[16] Zhang, D., and D. Ionescu. 2006. Robust and Optimal Control of Packet Loss Probability. IEEE Global Telecommunications Conference (GLOBECOM '06): 1–5.

[17] Ge, M., M. S. Chiu, and Q. G. Wang 2002. Robust PID Controller Design via LMI Approach. *Journal of Process Control*. 12(1): 3–13.

[18] Peaucelle, D. 2009. Integral Quadratic Separation Applied to Polytopic Systems. IFAC Symposium on Robust Control Design. Haifa.

[19] Çimen, T. 2012. Survey of State-dependent Riccati Equation in Nonlinear Optimal Feedback Control Synthesis. *Journal of Guidance, Control, and Dynamics*. 35(4): 1025–1047.

[20] Utkin, V. I. 1992. *Sliding Modes in Control and Optimization*. Springer-Verlag.

[21] Chilali, M., and P. Gahinet. 1996. H∞ Design with Pole Placement Constraints: An LMI approach. *IEEE Transactions on Automatic Control*. 41(3): 358–367.

[22] Slotine, J. J. E., W. Li, and others. 1991. *Applied Nonlinear Control*. New Jersey: Prentice-Hall.

[23] Hibbeler, R. C. 2013. *Engineering Mechanics: Statics*. New Jersey: Pearson Prentice Hall.